Int. J. Multiphase Flow Vol. 14, No. 2, pp. 155–174, 1988
Printed in Great Britain.

0301-9322/88 $3.00 + 0.00

CRITICAL TWO-PHASE FLOW THROUGH ROUGH SLITS

H. JOHN,[1] J. REIMANN,[1] F. WESTPHAL[2] and L. FRIEDEL[3]

[1]Kernforschungszentrum Karlsruhe, Institut für Reaktorbauelemente, Karlsruhe, B.R.D.

[2]Arbeitsgruppe Sicherheitstechnik, Universität Dortmund, Dortmund, B.R.D.

[3]Technische Prüfung, Hoechst AG, Frankfurt-Hoechst, B.R.D.

(*Received* 20 *March* 1987; *in revised form* 25 *October* 1987)

Abstract—Knowledge of the two-phase mass flow rate through a crack in the wall of nuclear or chemical reactor components is very important under the leak-before-break criterion point of view. For providing a qualified analytical tool for calculating critical mass flow rates through such a crack, a detailed test program was carried out using subcooled water up to pressures of 14 MPa. A real crack and several simulated cracks (rough slits) were examined experimentally. The important parameters such as inlet pressure, subcooling temperature of water, slit width and inner surface roughness were varied in a wide range and the measured data compared with calculated values from different models. The data comparison indicates that the model published by Pana leads to predictions which agree quite well with the observed data. First calculations were carried out using the friction coefficient ξ, which results from single-phase flow measurements. A correlation was developed to calculate ξ from the geometrical dimensions of the crack and was integrated into an advanced version of the Pana Model. The Modified Pana Model was qualified against some hundreds of test values. The measured data were predicted with a relative standard deviation of $<20\%$.

1. INTRODUCTION

In nuclear and chemical reactor safety the accurate prediction of critical leakage rates through openings of different geometries, which may be caused by breaks or cracks, is of great importance. A large number of experimental and theoretical studies have been published in the literature. Most of the studies concentrate on opening dimensions of 1–10 cm dia, the results of which are very often then extrapolated to pipes with diameters of the order of 1 m. These investigations were based on the earlier assumption of a total pipe break associated with the loss-of-coolant accident. With respect to the wall material used now, a sudden rupture of a pipe is not expected. Today the leak-before-break criterion is generally accepted (Munz 1984).

Presently, the interest is concentrated on the flow through small leaks. In this work, therefore, the flow through rough walled slits is investigated with typical hydraulic diameters of about $d_H = 0.4$ mm and a channel length of $L = 46$ mm. These slits are characterized by a large L/d_H ratio but a relatively small transit time of a fluid particle, and a large wall roughness. The question whether previous models can be used under these conditions was discussed, for example, by Wallis (1980), Amos & Schrock (1983) and Reimann (1984): for ducts with large L/D ratios mechanical and thermodynamical equilibria between the phases are often assumed (homogeneous equilibrium model, HEM). On the other hand, one can argue that the flow is characterized more by a thermodynamic non-equilibrium due to the small absolute flow length and short residence time. Therefore, models such as the Henry Model (Henry 1970a,b; Henry & Fauske 1971) should be appropriate. In this paper representative models of each group will be compared with the experimental results: the equilibrium model developed by Pana (1975, 1976); Model II of Abdollahian (1983, 1984); and the non-equilibrium Model I of Abdollahian, which is based on the Henry Model.

Previous experiments are rare and concentrated on slits with smooth walls or small roughnesses. Collier *et al.* (1980, 1984), Amos & Schrock (1983) and Kefer *et al.* (1986) performed experiments on slits using subcooled water and compared the results with models developed or modified by them. Table 1 shows the main parameters of these experiments.

In this study the range of parameters is much more extended and includes slits of different hydraulic diameters and artificially produced roughnesses (simulated cracks) and a real crack. For more details of this investigation reference is made to the work of John *et al.* (1987).

Table 1. Parameter range of the experiments

Authors	Fluid	Slit breadth Inlet (mm)	Slit breadth Exit (mm)	Slit depth, L (mm)	Slit width, S (mm)	Roughness, R (μm)	
Amos & Schrock (1983)	Subcooled H_2O $\Delta T = 0$–65 K $p_{max} = 16.0$ MPa	20.4	20.4	60–75 $A = 2.6$–7.8 mm^2	0.127 0.254 0.381		Simulated cracks
Collier *et al.* (1980)	Subcooled H_2O $\Delta T = 33$–120 K $p_{max} = 11.5$ MPa	57.2	57.2	63.5 $A = 11.4$–64 mm^2	0.2–1.12	0.3–10.2	Simulated cracks
Collier *et al.* (1984)	Subcooled H_2O $\Delta T = 0$–72 K $p_{max} = 11.5$ MPa	0.74–27.9	0.74–27.9	20 $A = 0.015$–6.55 mm^2	0.02 0.05 0.074 0.108 0.22	1.78	Real cracks
Kefer *et al.* (1986)	Subcooled H_2O $\Delta T = 0$–60 K $p_{max} = 16.0$ MPa	19–108	19–108	10–33 $A = 5.89$–13.93 mm^2	0.097 0.129 0.325	20–40	Simulated and real cracks

2. EXPERIMENTAL FACILITY

2.1. Test loop

Figure 1 shows a schematic view of the test loop. A steam-boiler system that can be operated at variable temperatures below saturation up to a maximum pressure of 14 MPa produces the subcooled water. To prevent obstruction of the narrow slits in the test section by corrosion product particles, the water passes a sintered metal filter before it flows through the variable orifice to the pressure vessel containing the test section. Downstream of the pressure vessel the fluid flows through a backpressure control valve and then into the condenser from which it is pumped back to the boiler. The pipes in the boiler system are fabricated from carbon steel and the pipes and container between the filter and backpressure valve are made of stainless steel. The loop is designed for 25 MPa nominal pressure. The stagnation pressure upstream of the test section is controlled by a bypass valve. The variable orifice for measurement of the single-phase water flow has 12 calibrated positions for the precise determination of the mass flow rate over a wide range of 0.01–3 kg/s. A differential pressure and several absolute pressure values, as well as several thermocouple signals, are used to define the property values for calculating the mass flow rate, the flow conditions upstream and downstream of the test section (p_0, T_0, p_u, ΔT) and the pressures in the slit. An on-line computer PDP 11–23 calculates the mass flow rates and subcooling temperatures and converts all important values into engineering units. These data are stored on a disk and printed out on a terminal for further data processing as well as for controlling the experimental procedure.

2.2. Test section

Figure 2 shows details of the test section. It is fixed on a circular plate with an 80 mm dia hole in the centre, which is flanged between the upper and lower parts of the pressure vessel. Two blocks of steel are mounted with a clamp on the plate with a rectangular slit in between. Two spacers, which can be replaced by others of varying thicknesses in steps of 0.1 mm limit the slit on two sides at 90° to the flow direction. The width of the slit was varied during the tests between about 0.2 and 0.6 mm, as will be described later. The depth of the slit was always 46 mm and the distance between the spacers 80 mm. By one set of screws the two blocks are pressed onto the sealing of the ground plate and by another set of screws in the clamp the blocks are pressed together against the spacers. Other screws press the spacers against their sealing surfaces. Pressure taps are used to measure the pressure gradient along the slit depth. The surface roughness of the two sides facing the slit were varied several times by shot blasting with sand and steel grit.

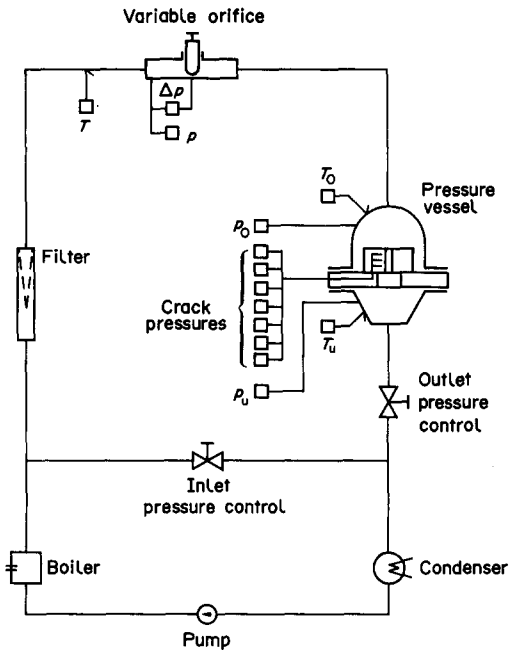

Figure 1. Schematic of the test loop.

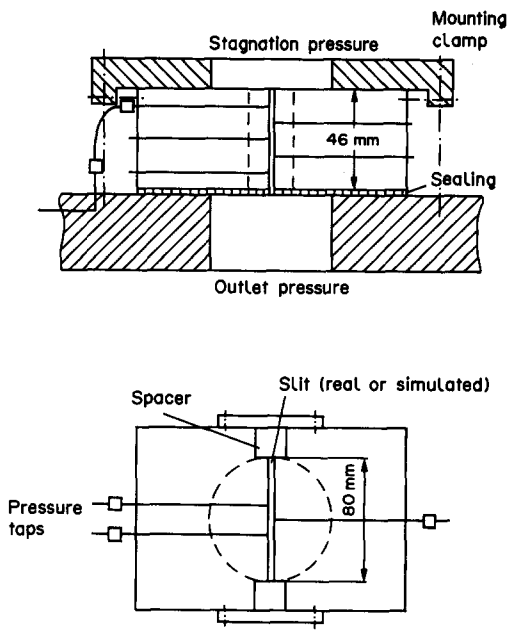

Figure 2. Test section with variable slit.

The two steel blocks used for the simulated cracks are made of stainless steel, while another steel block with the same geometrical dimensions was made of reactor pipe steel (20MnMoNi55) and had a real crack. The real crack was produced by cyclic bending on a material testing machine (Müller *et al.* 1986). Although the steel block was notched circumferentially before treating it, several samples had to be produced to obtain one usable crack which was fairly plain and parallel with defined dimensions. After breaking of the block the two grooves for the spacers were machined with the crack in the closed condition. The roughness of the surfaces in the simulated and the real cracks were measured with a perthometer (profilometer). The differences between the highest and lowest levels on the surface over a measuring length of about 5–10 mm were measured about 10 times on each side of the slit and the average of these results was defined as the roughness R. This definition of the surface roughness, which can be considered as an "averaged" peak-to-valley distance, is similar to that used for the definition of sand roughness by Nikuradse (1933) in his experiments. The high accuracy of calculations obtained using this definition (see subsection 4.3) justifies this choice. Several authors have used the so-called average roughness related to an average line of the peaks and valleys for the calculation of the fluid friction. Following this definition, smaller values of roughness are obtained. Indeed this choice seems to be misleading because very low peaks occurring between high ones can considerably influence the value of this parameter but have only a small effect on the real friction.

The determination of the crack width, which is used for the evaluation of the effective cross section of the flow and the hydraulic diameter, is also associated with some uncertainties. After mounting the test section on the basic plate, the inlet and the outlet width of the slits were measured with gauges, available in steps of thickness of 0.01 mm. The amount of the roughness R (two times 1/2 roughness) was added to this measured distance of the roughness peaks S_m to obtain the effective width of the slit $S = S_m + R$.

In some cases it happened that the slit outlet width was slightly larger than the inlet dimension. This was probably caused by small deformations of the test section as a result of mounting forces. In these cases, the outlet dimensions are used for all calculations, taking into account the higher velocity at the outlet. Due to a small waviness of the surfaces of the real crack, a different method was applied for defining the crack width. At first, the machined grooves for the spacers were measured in the closed condition, where the surfaces were in contact with each other. Then, the spacers were fabricated with thicknesses of 0.1, 0.2 and 0.3 mm larger. Again the roughness R was

Table 2. Dimensions of the tested slits (cracks)

Sample No.	Total slit entrance (mm)	Width of exit (mm)	Roughness (μm)	Cross-section A_c (mm^2)	Friction factor ξ_{sc}
2.204	0.205	0.25	5	20.0	3.2
2.13A	0.25	0.35	70	28.0	18.1
2.24A	0.26	0.26	70	20.8	23.0
3.13A	0.27	0.35	70	28.0	15.3
3.24A	0.34	0.39	70	31.2	8.1
3.13B	0.34	0.43	150	34.4	15.2
3.24B	0.41	0.48	150	38.4	11.2
2.13B	0.24	0.32	150	25.6	38.2
4.24B	0.53	0.58	150	46.4	8.3
†2.15R	0.44	0.44	240	35.2	85
†3.15R	0.54	0.54	240	43.2	43
†4.15R	0.64	0.64	240	51.2	23.5
2.24C	0.24	0.25	100	20.0	28.2
3.13C	0.39	0.43	100	34.4	7.8
4.13C	0.50	0.55	100	44.0	6.4
2.24D	0.21	0.28	50	22.4	7.5

†Real cracks.

added to these values because it was not expected that the peaks and valleys of the surface roughness would overlap exactly in the zero position. Table 2 contains the main dimensions of 13 simulated and 3 real crack configurations.

2.3. Test procedure

Figure 3 shows the test matrix of the experiments. Most tests were performed at pressures p_0 of 4, 6, 8, 10 and 12 MPa and a few at 14 MPa. Subcooling temperatures ΔT were 60, 50, 40, 30, 20, 10 and 2 K. For zero subcooling the stability of the test loop could not be attained. A total number of 458 test points were obtained.

The main parameters for the test procedure were initial stagnation pressure p_0, temperature T_0 and backpressure p_u. After starting up the boiler, the pipe system was heated and cleaned by letting the hot water flow through to the test section in the condenser. Normally, the test series started at the lowest pressure and lowest temperature value ($p_0 = 4$ MPa, $\Delta T = 60$ K). While the temperature of the boiler continuously increased, the stagnation pressure was kept constant by control by the bypass valve. The time necessary to proceed from one point to the next was about

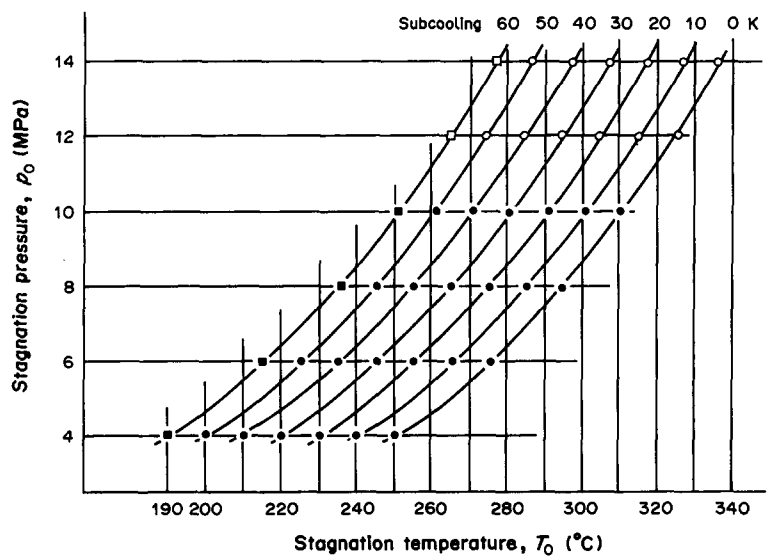

Figure 3. Test matrix for each slit geometry.

20–30 min. The backpressure was varied only for those points at the maximum subcooling temperature ($\Delta T = 60$ K) and for some at 10 K subcooling temperature. By closing the backpressure valve, the subcritical pressure in the slit outlet was reached and several single-phase pressure drop measurements were performed. The measurements at $\Delta T = 60$ K were used to calculate the single-phase friction coefficient ξ at test temperatures; ξ was calculated immediately after having taken the experimental values. This was necessary for checking, since the consistency of these values over the whole test run was an indication that the geometry of the slit remained constant, and no obstruction occurred. The definition of ξ and more details of its determination are given in subsection 4.1.

3. MODELS CONSIDERED FOR THE CRITICAL MASS FLOW RATE

The main goal of this investigation is to find a model to predict accurately the mass flow rate. Four models were selected and will be briefly described below. Two of these models are based on the measured single-phase friction coefficient ξ. Thus, the uncertainty of the definition of the geometric crack parameters is eliminated. Later on, the Pana Model will be extended by our own correlation for ξ and the slit parameters introduced in the calculation.

3.1. Pana Model

Pana (1975, 1976) proposed a model for calculating the critical mass flow rates with subcooled and saturated water, taking into consideration the fluid friction in the slit. It is based on thermodynamic equilibrium models such as the modified Bernoulli equation and the HEM or alternatively, the Moody Model (Moody 1965). For leaks through narrow cracks where the flow is well-mixed and has almost no slip, the HEM is realistic; while for large openings like a pipe break, the Moody Model—based on the presence of phase slip—is applicable. In the range of our test parameters, the Moody Model would give 30–100% higher mass flow rates than the experiments and in this respect it is unrealistic. The Pana Model divides the range of expansion from subcooled water to critical two-phase flow into two parts. This is illustrated by the enthalpy–entropy diagram shown in figure 4. Rising from low to higher temperatures at constant pressure p_0, the first region begins at the temperature T_0'' as the inlet condition where just critical flow condition begins and the fluid in the channel exit reaches the saturation line of the water at the backpressure p_u. With increasing temperature T_0 the exit pressure p_2 increases but remains on the saturation line

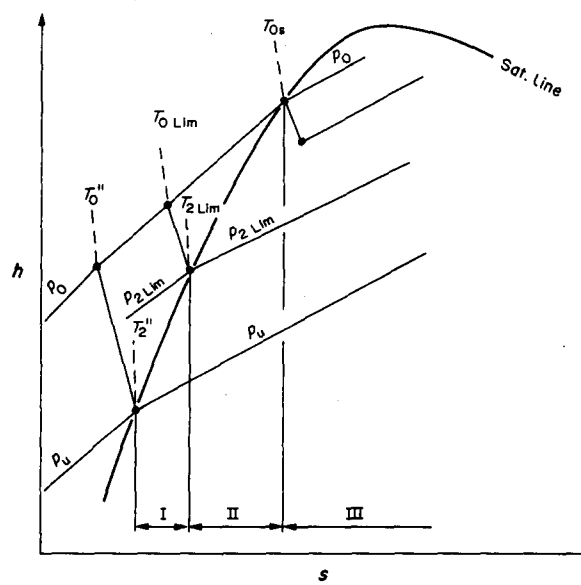

Figure 4. Enthalpy–entropy diagram for the description of the Pana Model.

($p_2 > p_u$). Region I ends when the inlet temperature reaches $T_0 = T_{0\,\mathrm{lim}}$ and flashing in the exit cross section of the slit starts to proceed upstream with decreasing subcooling. Region II begins at $T_0 = T_{0\,\mathrm{lim}}$ with two-phase flow at the exit and a noticeable steam content. With increasing temperature T_0, the point of flashing onset in the slit migrates from the exit in the direction of the inlet. The flashing point ends in the slit inlet, when the stagnation conditions reach saturation $T_0 = T_{0s}$ (subcooling $\Delta T = 0$). Region III begins with two-phase flow ($x \neq 0$) in the inlet. However, this region is not of interest in this study. The extent of the regions is dependent on the inlet pressure p_0 and the friction factor ξ.

For each region Pana provides equations for the determination of the mass flux.

Region I:

$$G = \left[\frac{2(p_0 - p_2)}{v(1+\xi)}\right]^{0.5}. \qquad [1]$$

In this equation, p_2 is the saturation pressure at T_2 and v is the specific volume. As the temperature difference $T_0 - T_2$ is very small, the Bernoulli equation can be approximated by

$$G \approx \left[\frac{2[p_0 - p_s(T_0)]}{v_s(T_0)\cdot(1+\xi)}\right]^{0.5}. \qquad [2]$$

This modified Bernoulli equation is very easy to handle. It reveals that the driving force for the mass flux is the pressure difference between the inlet pressure and the saturation pressure at the inlet temperature. The limit of validity of [2] is reached if $G = G_{\mathrm{lim}}$ and

$$\left.\frac{p_0}{p_s(T_0)}\right|_{\mathrm{lim}} = 1 + \frac{1+\xi}{2}\cdot\frac{G_{\mathrm{lim}}\cdot v_s}{p_s}. \qquad [3]$$

Region II. If

$$\frac{p_0}{p_s(T_0)} < \left.\frac{p_0}{p_s(T_0)}\right|_{\mathrm{lim}}, \qquad [4]$$

the actual flow conditions are in Region II. The mass fluxes in this region are limited on the one side by G_{lim} as a function of $T_{0\,\mathrm{lim}}$ and $T_{2\,\mathrm{lim}}$, with $x_2 = 0$ at $T_{2\,\mathrm{lim}}$, and on the other side by $G_{2\mathrm{ph}}$ as a function of T_{0s} and the condition $x_0 = 0$ at T_0 and $\Delta T = 0$. For the calculation of G_{lim} and the $G_{2\mathrm{ph}}$ the HEM is used.

In Region II, Pana assumed the mass flux G to be a linear function of the temperature T_0. It decreases from G_{lim} to G_{HEM}, while the temperature increases from $T_{0\,\mathrm{lim}}$ to T_{0s}:

$$G = G_{\mathrm{HEM}} + \frac{T_{0s} - T_0}{T_{0s} - T_{0\,\mathrm{lim}}}\cdot(G_{\mathrm{lim}} - G_{\mathrm{HEM}}). \qquad [5]$$

The critical mass flow is based on the assumptions of no slip between the phases and thermodynamic equilibrium (saturation temperature for both water and steam). Pana further assumed isentropic inlet flow (position 0 to 1), e.g.

$$s_0 = s_1 = x_1 s_{G1} + (1 - x_1)s_{L1}. \qquad [6]$$

Herewith, s and x denote the entropy and the stream quality, the subscrips L and G represent the liquid and the gas phases and 0 and 1 denote the location upstream and in the inlet, respectively.

The energy balance between 0 and 2 gives

$$G = \left[\frac{2[h_0 - (1-x_2)h_{L2} - x_2 h_{G2}]}{[x_2\cdot v_{G2} + (1-x_2)v_{L2}}\right]^{0.5}, \qquad [7]$$

where v is the specific volume and h is the enthalpy. The momentum balance between 1 and 2 yields

$$\xi = \int_{p_1}^{p_2} -2\frac{1 + G^2\dfrac{\mathrm{d}v}{\mathrm{d}p}}{G^2\cdot v}\cdot\mathrm{d}p = f(G_1, G_2, p_1, p_2, x_1, x_2), \qquad [8]$$

with

$$\frac{dG}{dp} = 0 \qquad [9]$$

the critical mass flow is calculated.

G_{lim} and G_{HEM} are calculated by an iterative procedure from these equations.

For determination of $G_{lim} = f(T_{2\,lim})$ the temperature $T_{2\,lim}$ also has to be calculated:

$$T_{0\,lim} - T_{2\,lim} = \frac{[v(T_{2\,lim}) \cdot G_{lim}(T_{2\,lim})]^2}{C_p(T_{2\,lim})} \cdot \frac{1+\xi}{2} \cdot \left(\alpha \cdot T_2 - \frac{\xi}{1+\xi}\right), \qquad [10]$$

where

$$C_p = \left|\frac{dh}{dT}\right|_p \qquad [11]$$

and

$$\alpha = \frac{1}{v} \cdot \left|\frac{dv}{dT}\right|_p. \qquad [12]$$

This equation is also solved iteratively.

3.2. Abdollahian Model I

This model is based on Henry's (1970a,b) non-equilibrium critical flow model; a homogeneous (no slip) flow is assumed. Thermodynamic non-equilibrium effects are introduced through an empirical parameter N, which is a function of the equilibrium quality and the flow path length/hydraulic diameter ratio. Additionally, the Henry Model was empirically extended by including the pressure drop along the flow path. The pressure drop across the crack is calculated as the sum of pressure drop components, according to

$$\Delta p_{tot} = \Delta p_e + \Delta p_f + \Delta p_A + \Delta p_{AA}, \qquad [13]$$

where

$$\Delta p_e = \frac{G_C^2 \cdot v_{L0}}{2C^2} \qquad [14]$$

is the entrance pressure loss with the orifice contraction coefficient C ($C = 0.61$). The friction pressure drop is

$$\Delta p_f = \frac{12}{2} \cdot \lambda \cdot G_C^2 \cdot v_{L0} + \lambda \frac{\frac{L}{d_H} - 12}{2} \cdot G_C^2 [v_L + x(v_G - v_L)], \qquad [15]$$

with the friction factor λ calculated from the modified Karman correlation:

$$\lambda = \left(2 \log \frac{d_H}{2K} + 1.74\right)^{-2}, \qquad [16]$$

where K is the average roughness height. ΔP_A and ΔP_{AA} are the pressure drops due to area change and due to phase change. The critical pressure p_c is the difference between the stagnation pressure p_0 and the total pressure difference ΔP_{tot}; the critical mass flux is calculated according to Henry by

$$G_c^2 = \left[x \frac{v_G}{\kappa \cdot p_c} - (v_G - v_{L0}) \cdot N \frac{dx_E}{dp}\right]^{-1} \qquad [17]$$

and the assumption

$N = 20x_E$ if $x_E < 0.05$ and $N = 1$ if $x_E \geqslant 0.05$, where x_E is the equilibrium quality and κ is the isentropic exponent.

For the first comparative calculations with the Pana Model this model was modified by substitution of [13] by

$$\Delta p_{tot} = (1 + \xi) \cdot \frac{v_{L0}}{2} \cdot G_C^2 \qquad [18]$$

This version is termed the Modified LEAK-01 Model hereafter.

3.3. Abdollahian Model II

Abdollahian (1983, 1984) suggested a simplified homogeneous equilibrium model for subcooled upstream conditions. It is a simplified closed-form relationship and, in contrast to Model I, it does not require details of the flow path geometry as input variables.

With the main assumption that $p_c \approx p_s(T_0)$ and considering only entrance and friction losses, the critical mass flux can be obtained from the following relations:

$$G_c = \left[\frac{2[p_0 - p_s(T_0)}{v_m + v_m \cdot f \cdot \frac{L}{d_H} + \frac{v_0}{C^2}} \right]^{0.5}, \qquad [19]$$

where $C = 0.61$; and

$$v_m = \bar{v}_L + \bar{x} \cdot (\bar{v}_G - \bar{v}_L), \qquad [20]$$

where $\bar{v}_L$ and $\bar{v}_G$ are the average liquid and vapour specific volumes and $\bar{x}$ is the average enthalpic mass flow quality.

3.4. Collier Model

The model published by Collier *et al.* (1980), like the Abdollahian Model I described in subsection 3.2, is based on Henry's (1970) non-equilibrium critical flow model. The main difference between both models is the equation used for determination of the pressure loss due to friction.

Instead of [15], Collier *et al.* introduced in their model the following correlation:

$$\Delta p_f = \frac{\lambda}{4} \left(\frac{L}{d_H} - 12 \right) \cdot G_c^2 \left[v_L \left(1 + \frac{A_e^2}{A_i^2} \right) + x_e (x_{Gc} - v_{L0}) \right], \qquad [21]$$

where the subscripts c, e and i represent the critical condition, exit and the location $L/d_H = 12$, respectively.

4. RESULTS

4.1. Measurement of the friction coefficient

The friction coefficient for single-phase flow is defined as

$$\xi_e = \frac{2 \cdot (p_0 - p_u) A_e^2 \cdot \rho}{\dot{m}^2} - 1. \qquad [22]$$

Here ρ is the average density, $\dot{m}$ is the measured mass flow rate, p_0 ans p_u are the stagnant pressures upstream of the inlet and downstream of the exit and A_e is the cross-section of the exit. The entrance pressure loss as well as the influence of the cross-section variation on the pressure loss are included in ξ_e. The friction coefficient was slightly dependent on the temperature T_0 and the pressure difference $(p_0 - p_u)$, which is probably caused by small deformations of the test section. Therefore, many measurements were performed and several repeated to obtain a reasonable averaged value. The arithmetic deviation of the ξ_e values from the average was about 5–8%. Test points with a higher deviation were rejected. The values listed in table 2 are average values. Measurements which were made with cold water (70°C) produced 10–20% higher ξ_e values. Therefore, only values measured at temperatures which were close to the two-phase flow conditions were used for the calculations.

4.2. Correlation for calculating the friction coefficient from the crack dimensions

The determination of the friction coefficient experimentally, as described in subsections 2.2 and 4.1, is not possible in general. Usually, only the geometrical dimensions of the crack are known,

sometimes from a crack growth calculation. For an application of the chosen model, a correlation for the single-phase friction coefficient must be available.

We propose

$$\xi_e = \xi_i + \xi_f + \xi_E, \qquad [23]$$

where ξ_i is the inlet loss, ξ_f is the friction loss and ξ_E is the exit loss.

For sharp-edged inlets a value of $\xi_i = 0.5$ is recommended (VDI-Wärmeatlas 1984).

The friction loss is given by

$$\xi_f = \lambda \cdot \frac{L}{d_H}, \qquad [24]$$

with the friction factor λ, the flow length L and the hydraulic diameter of the slit $d_H = 2S_A$.

The exit loss is neglected. Several empirical expressions for the friction factor λ can be found in the literature, usually they are based on experiments with ducts or pipes of larger dimensions. Nikuradse (1933) showed in his classic diagram that the friction loss in a rough pipe for high Reynolds numbers is only dependent on the hydraulic diameter/surface roughness ratio. For this region Nikuradse developed an expression of the type

$$\lambda = \left(a \cdot \log \frac{d_H}{R} + b\right)^{-2}. \qquad [25]$$

The coefficients a and b were determined to be 2 and 1.14, respectively. Button *et al.* (1978) confirmed this type of equation by experimental work on narrow rough slits and proposed the values $a = 2.25$ and $b = 1.25$. In our experiments, the single-phase friction loss was also no longer dependent on the Reynolds number. From [23], [24] and $\xi_i = 0.5$ we obtain

$$\lambda = \left(3.39 \cdot \log \frac{d_H}{R} - 0.866\right)^{-2}. \qquad [26]$$

In figure 5, the correlations of Nikuradse (1933) and Button *et al.* (1978) are displayed. It can be seen that our results are between these functions.

The equation for the friction coefficient ξ_e reads, finally,

$$\xi_e = 0.5 + \left(3.39 \cdot \log \frac{d_H}{R} - 0.866\right)^{-2} \cdot \frac{L}{d_H}. \qquad [27]$$

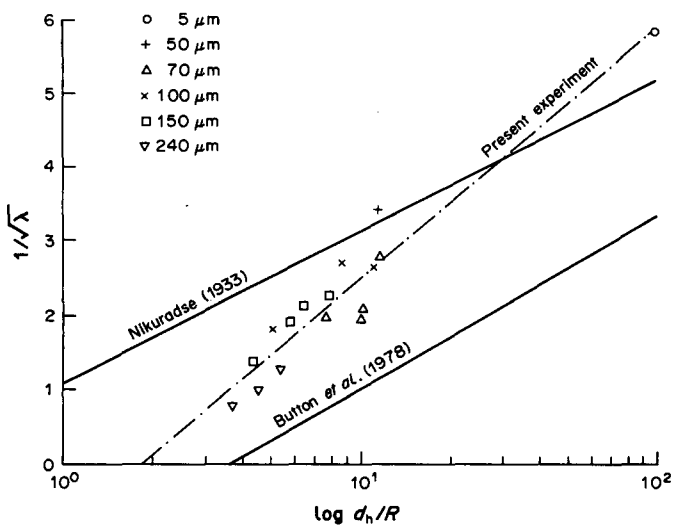

Figure 5. Friction factor as a function of slit geometry.

Equation [27] is combined with the Pana Model. Hereafter it is called the Modified Pana Model. It is only valid if the definitions for R and d described in subsection 2.1 are used.

4.3. *Critical mass flux data from experiments and calculations*

The measured mass flux is compared with predicted values according to the following models:

(a) Original Pana Model (subsection 3.1).
Modified LEAK-01 Model (subsection 3.2).
These models are combined with the measured friction coefficients.

(b) Modified Pana Model (subsection 4.2).
Abdollahian Model I (subsection 3.2).
Abdollahian Model II (subsection 3.3).
These models use only geometrical crack dimensions with pressure drop correlations.

(c) Collier Model (subsection 3.4).
This model is only used for the error analysis relating to the different data sets and different models.

Figures 6 and 7 show the measured mass flux as a function of the friction coefficient ζ, the inlet pressure p_0 and the subcooling temperature ΔT. The points can be fitted well by a set of curves which decrease with decreasing inlet pressure and increasing friction coefficient.

The curves traced for a subcooling temperature of 60 K (figure 7) are steeper than those for a subcooling temperature of 2 K (figure 6). These diagrams show that the friction coefficient is the governing parameter.

In figure 8 the mass flux is presented as a function of the L/d_H ratio with constant values for the surface roughness and inlet pressure. This type of presentation is often used in the literature. These curves are only comparable with those from other experiments when the definitions of crack geometry are identical. In addition, figure 8 presents the results of Collier *et al.* (1980). Indeed these values do not fit the systematic trends in our diagram, probably due to differences in the roughness definition.

In figures 9 and 10 the experimental results, together with the Pana Model predictions, are shown as a function of the subcooling temperature. The calculated values are close to the measured values, but are always slightly higher.

In figure 11 the ratio of calculated/measured mass flux G_c/G_m, according to the Pana Model, are plotted vs the subcooling temperature ΔT for one slit configuration. In figure 12 the

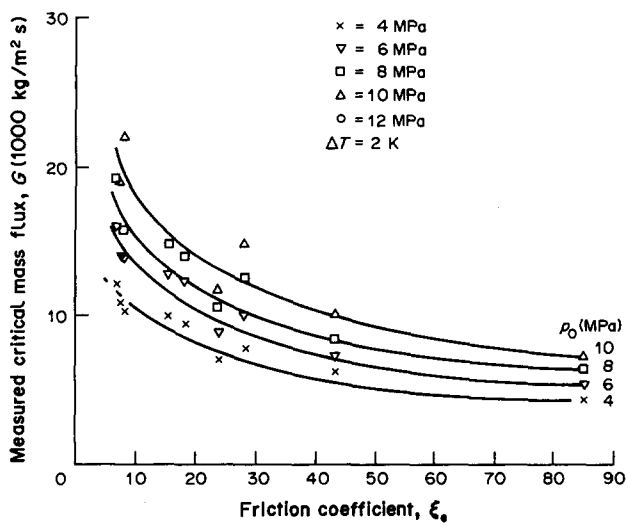

Figure 6. Critical mass flux as a function of the friction coefficient ζ_e (subcooling 2 K).

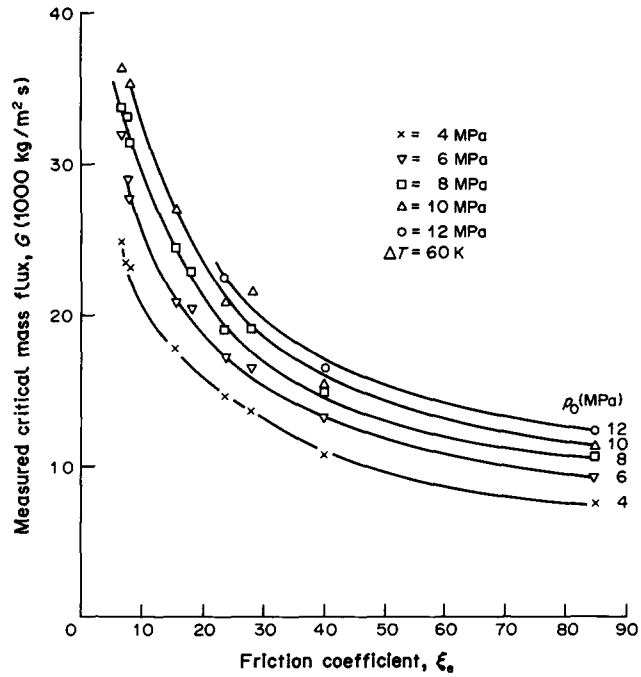

Figure 7. Critical mass flux as a function of the friction coefficient ξ_e (subcooling 60 K).

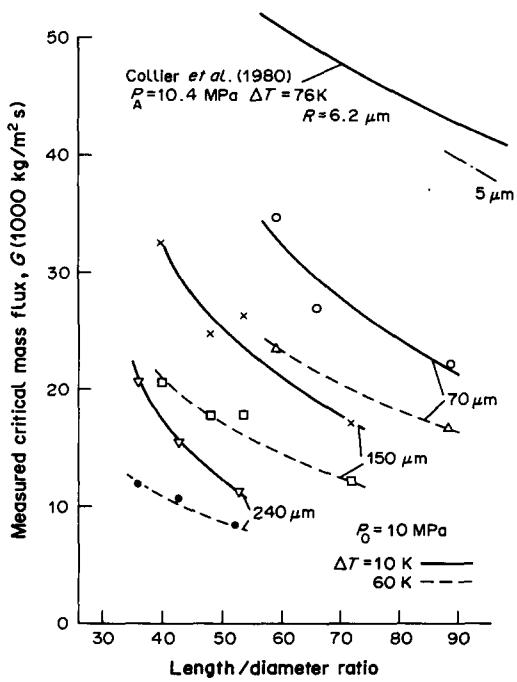

Figure 8. Critical mass flux as a function of L/d_H.

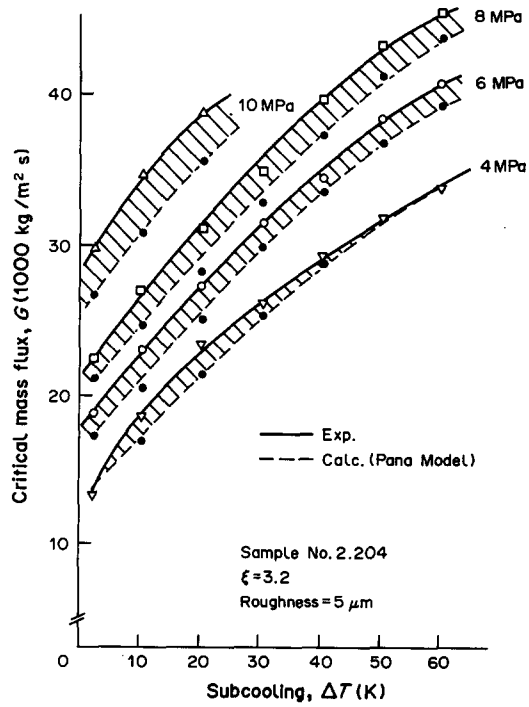

Figure 9. Critical mass flux as a function of subcooling ($\xi_e = 3.2$).

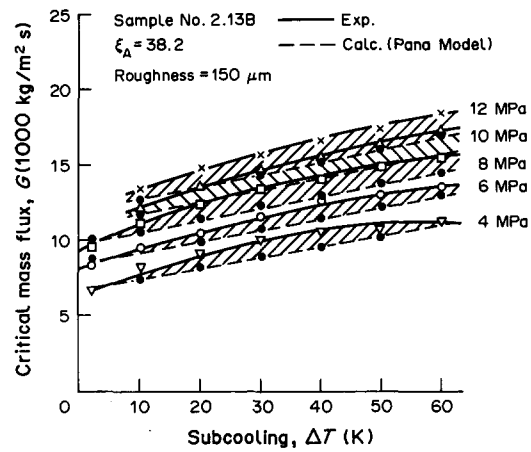

Figure 10. Mass flux as a function of subcooling ($\xi_e = 38.2$).

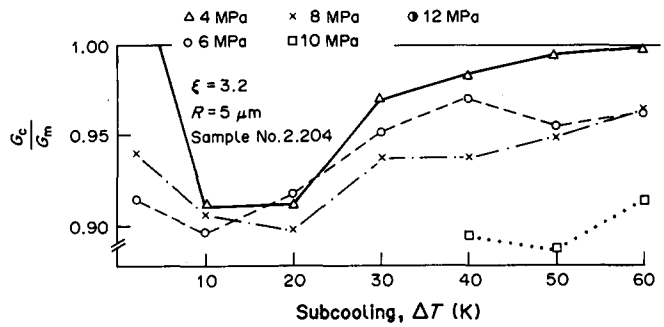

Figure 11. Ratio of calculated/measured critical mass flux (Pana Model).

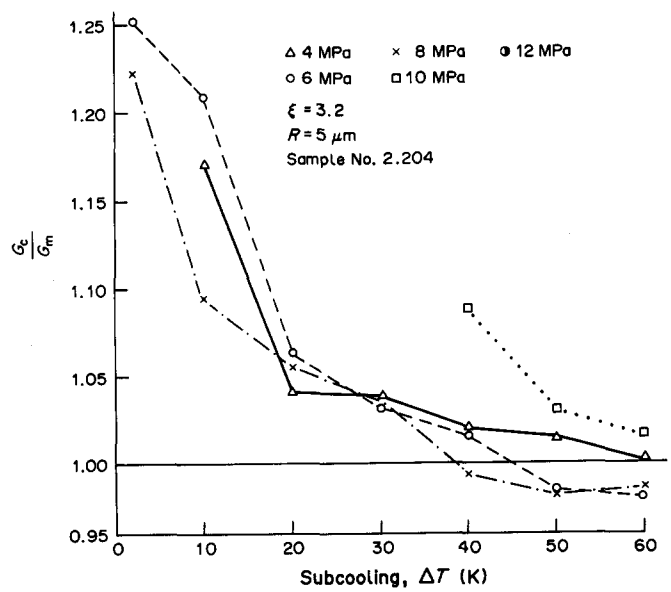

Figure 12. Ratio of calculated/measured critical mass flux (Modified LEAK-01 Model).

corresponding curves resulting from the Modified LEAK-01 Model are shown. It can be seen that the Pana Model predicted values are closer to the measured data than those of the Modified LEAK-01 Model. One reason for this could be that the equilibrium term in the Modified LEAK-01 Model, proposed by Henry (1970a,b), overpredicts the mass flux for this type of flow.

In figures 13(a,b) the total mass flux data (458 experimental points), measured using 16 different slit configurations (table 2), are compared with predictions from the Pana Model [figure 13(a)] and the Modified LEAK-01 Model [figure 13(b)].

We conclude that the Pana Model describes the experiment best with a relative standard deviation of 10.2%. The Modified LEAK-01 Model predictions show a larger deviation with a relative standard deviation of 16.3%.

For the analysis we used the following characteristic error numbers:

relative error,

$$\bar{X}_m = \frac{1}{n}\sum_{i=1}^{n} X_{im}, \qquad [28]$$

$$X_{im} = \frac{(G_{meas} - G_{calc})}{G_{meas}}; \qquad [29]$$

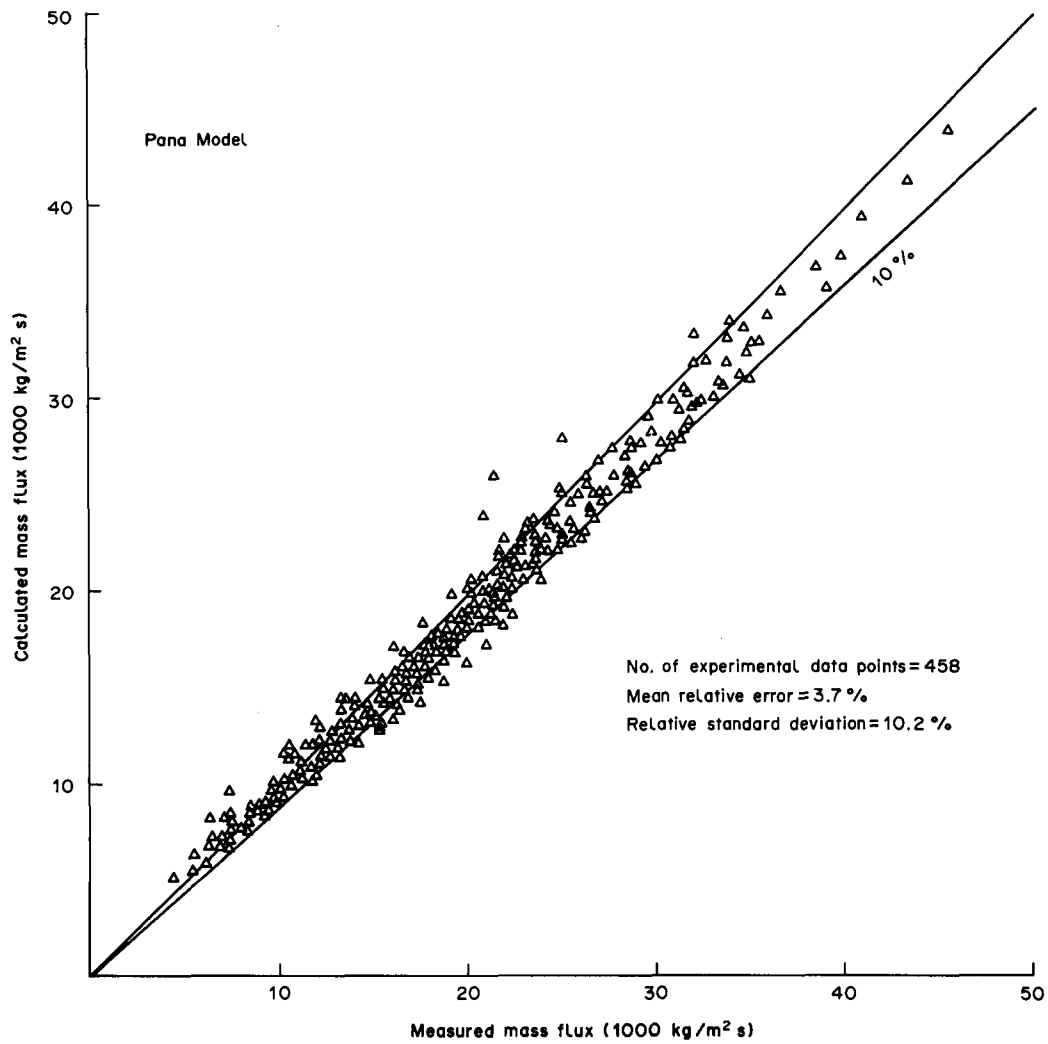

Figure 13(a)

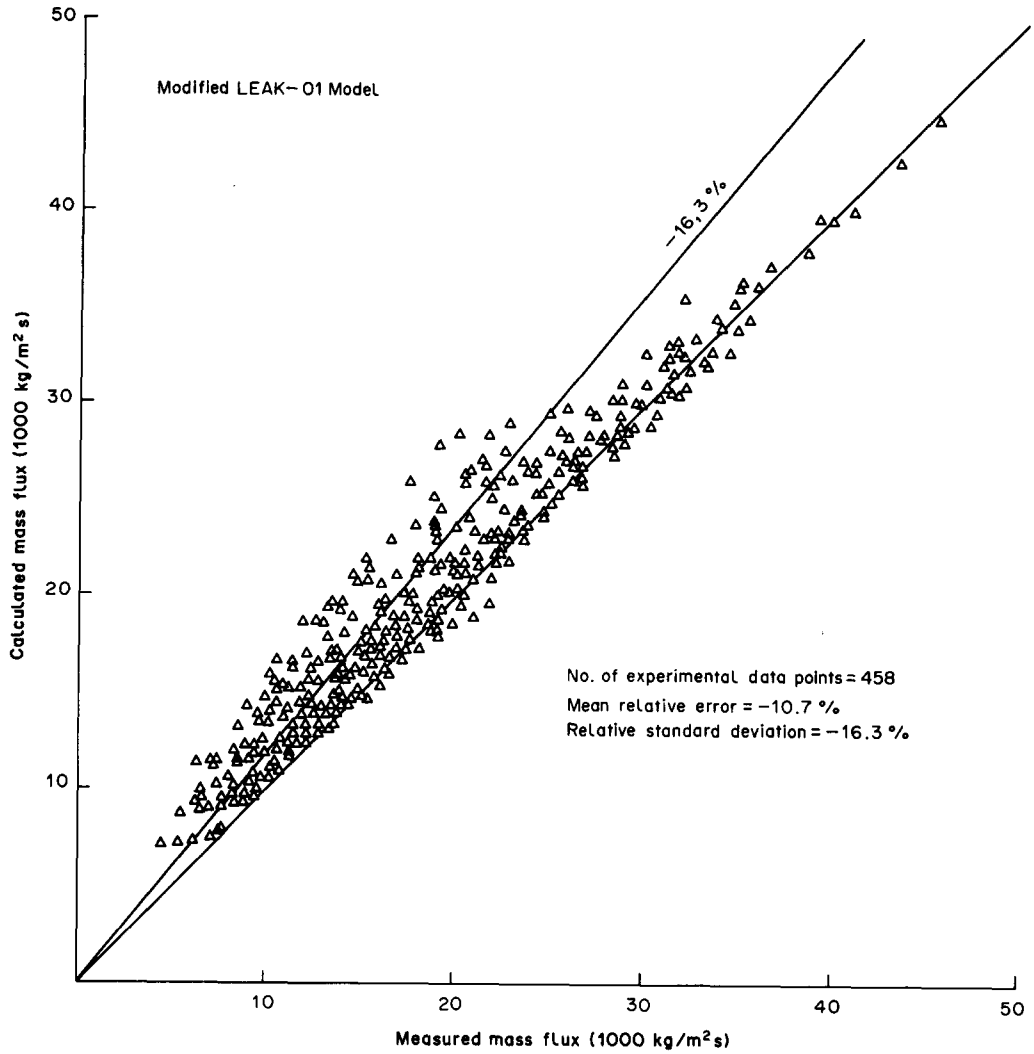

Figure 13(b)

Figures 13(a, b). Comparison between calculated critical mass flux (with use of measured ξ_e) and experimental values.

relative standard deviation,

$$S_{Rm} = \left[\sum_{i=1}^{n} \frac{X_{im}^2}{(n-f-1)} \right]^{0.5}, \qquad [30]$$

where n is the number of data and f is the number of variables in the models.

The comparison between experimental and analytical data obtained from the Modified Pana Model is shown in figure 14(a). Corresponding results obtained with the original Abdollahian Model I and the Abdollahian Model II are shown in figures 14(b) and 14(c), respectively. These calculations are carried out for the crack dimensions listed in table 2. It can be seen that the Modified Pana Model predictions exhibit greater scatter than the predictions according to the Pana Model [figure 13(a)]. It is assumed that the deviations are caused by the new correlation and the uncertainties in the surface roughness measurement. Comparing the predictions of the three models, the scattering range and the deviations are still smallest for the Modified Pana Model [figures 14(a)–(c)], confirming that the Pana Model and the Modified Pana Model predict our experiments best. If the type of crack is considered it is obvious that the mass flux in the real crack is larger than in the simulated cracks. This effect may be caused by the uncertainty in the determination of the width of the real cracks, as mentioned in subsection 2.2.

Figure 14(d) shows a comparison between experimental data obtained by Collier *et al.* (1980, 1984) and Amos & Schrock (1983) and values calculated with the Modified Pana Model. The results of the error analysis are listed in table 3. In table 3 all analytical data are summarized—having being calculated on the basis of the different models and data sets discussed or mentioned in this contribution. The results of the model proposed by Collier *et al.* (1980, 1984), are also included in this comparison.

The data from Amos & Schrock (1983), do not include the surface roughness required here for the analysis. They were calculated on the basis of the single-phase calibration data. The large deviation between the experiment and predictions of Collier *et al.* using the Modified Pana Model probably result from Collier's values for the surface roughness, which were probably defined as arithmetically averaged values. The peak-to-valley roughness of a surface is not a clear function of the "averaged roughness" because this is dependent on the character of the surface profile. By our perthometer measurements we found that the arithmetical average is about 8–10 times smaller than the peak-to-valley roughness. This observation was roughly confirmed by Button *et al.* (1978). If the roughness is increased by a factor of 8–10, using the diagrams plotted in figures 6 and 7 a mass flux can be estimated which is smaller by a factor of 1.3–3. This gives a possible explanation for the overprediction of the simulated values shown in figure 14(d) and table 3. The large

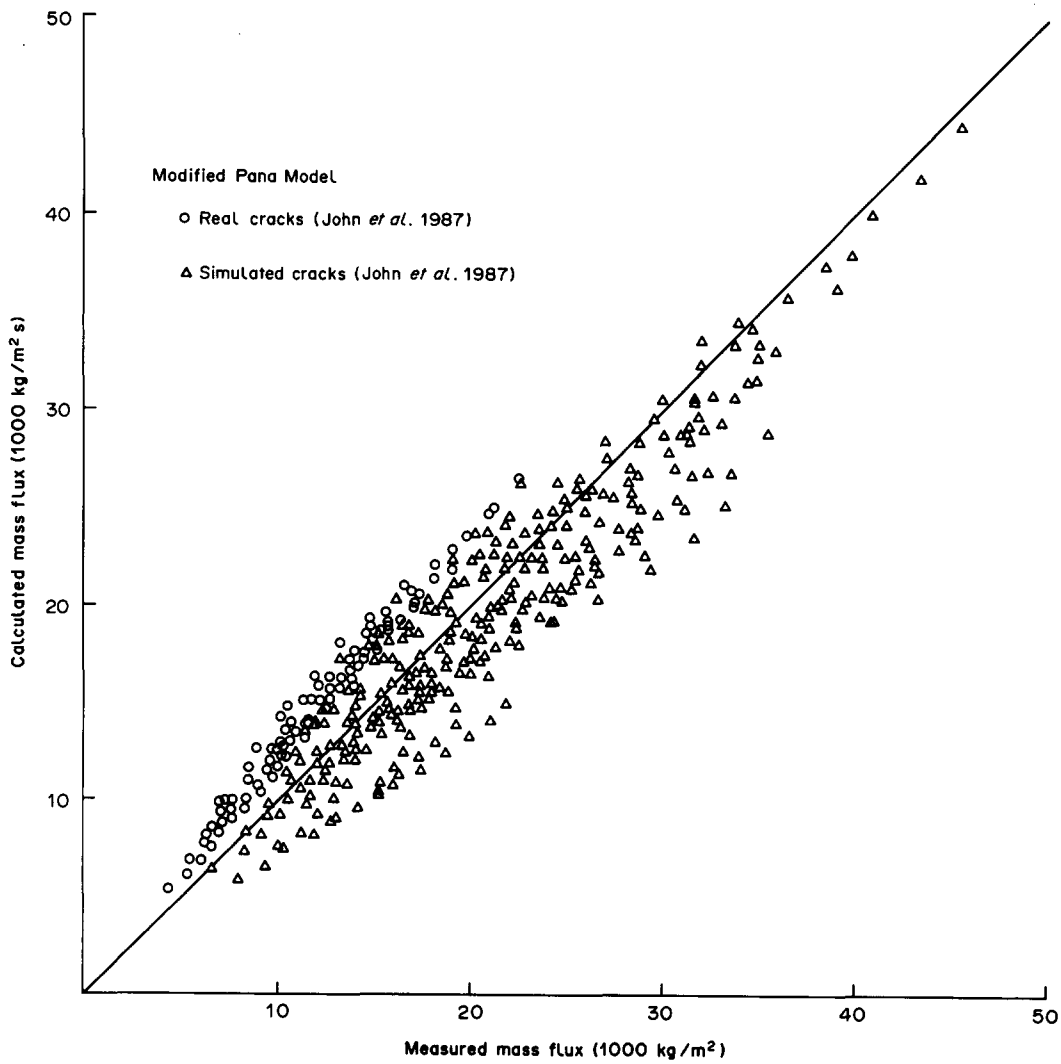

Figure 14(a)

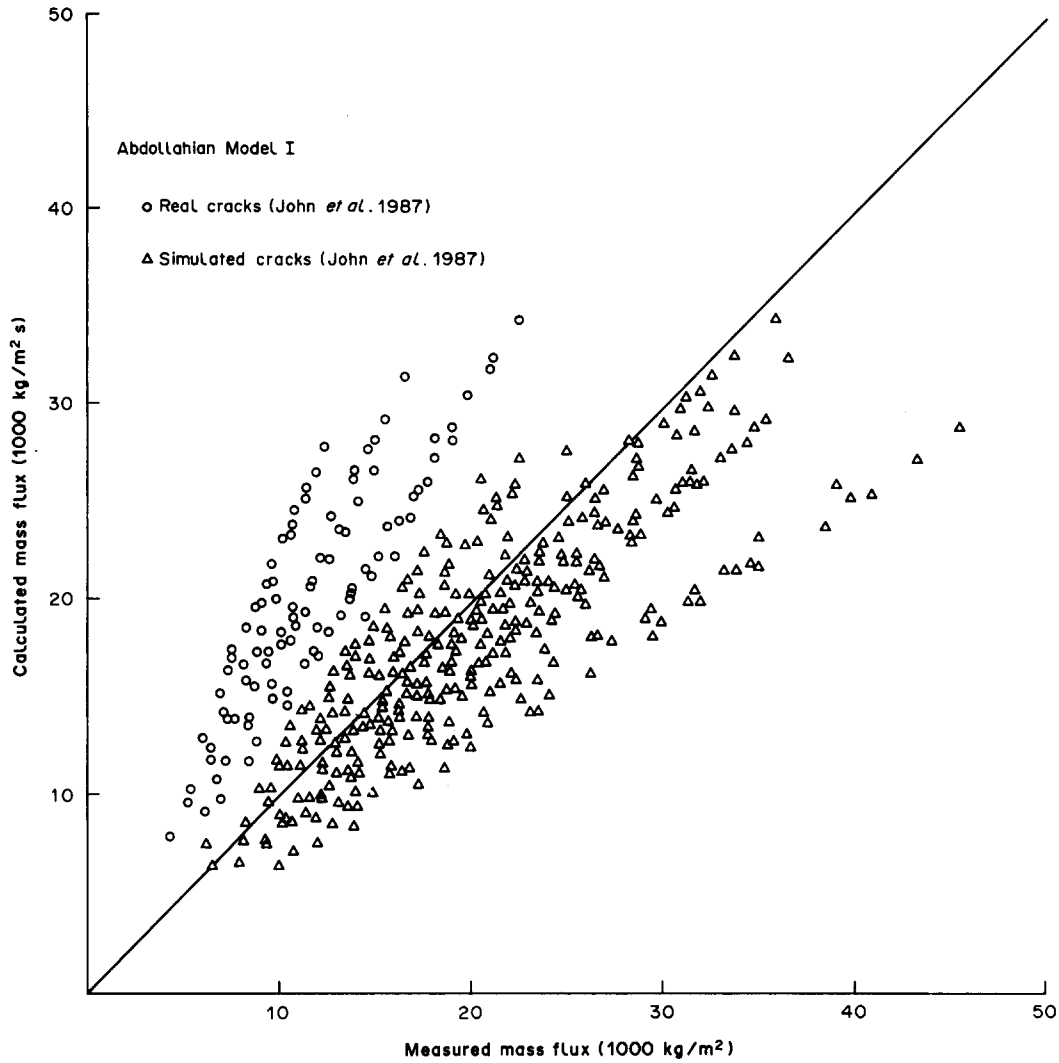
Abdollahian Model I
o Real cracks (John et al. 1987)
Δ Simulated cracks (John et al. 1987)
Calculated mass flux (1000 kg/m² s)
Measured mass flux (1000 kg/m²)
10
20
30
40
50

Figure 14(b)

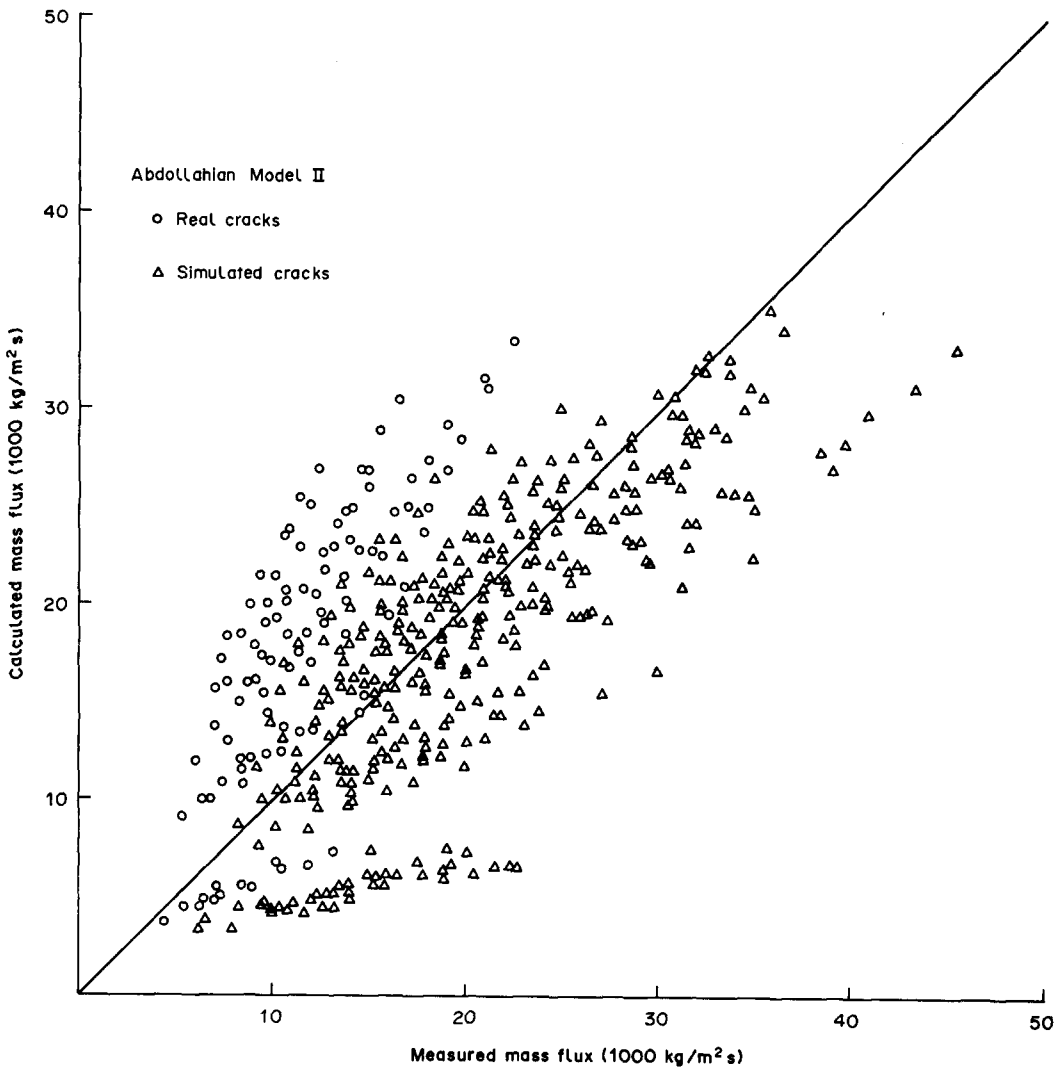
Abdollahian Model II
o Real cracks
Δ Simulated cracks
Calculated mass flux (1000 kg/m² s)
Measured mass flux (1000 kg/m² s)
10
20
30
40
50

Figure 14(c)

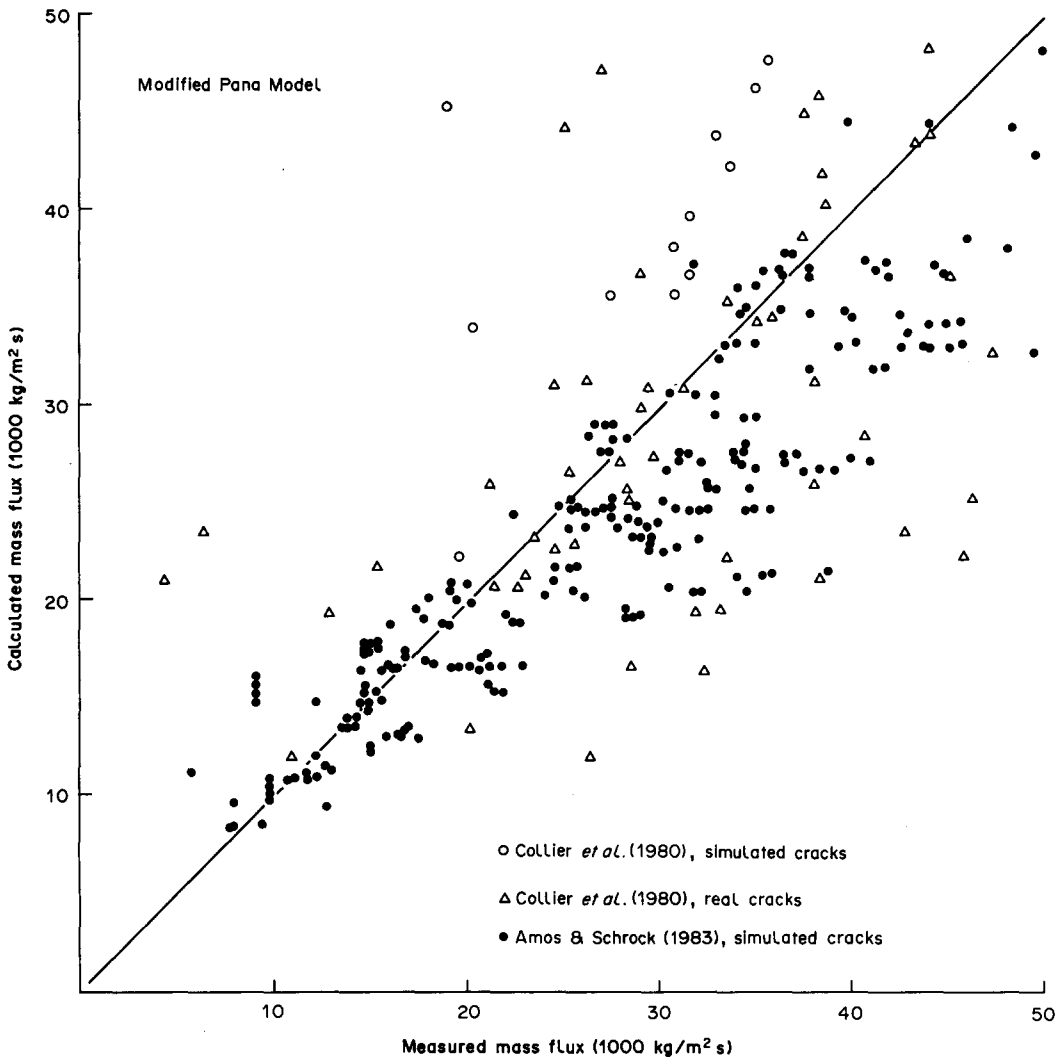

Figure 14(d)

Figures 14(a–d). Comparison between calculated critical mass flux (with use of crack dimensions) and experimental values.

deviation of the real crack data from Collier *et al.* in both directions can not be explained. Generally, these data (Phase II) indicate a very much higher scatter than the simulated data, probably caused by a less accurate determination of the slit dimensions.

5. CONCLUSIONS

The Modified Pana Model is proposed as a qualified analytical method for calculating steam–water leakage rates through cracks in the wall of a pressure vessel or in pipes. A reasonably good agreement of the observed and predicted data was found. This comparison demonstrates the capability of the model for prediction within an error of $<20\%$ related to the standard deviation. However, this method requires crack parameters, particularly the surface roughness, as defined, and that the crack shapes correspond roughly to those which were investigated experimentally.

The influence of surface roughness, crack width and thermodynamic parameters was examined systematically. However, the extent of the parameter range is still small, so excluding an extrapolation of the methodology to all shapes and geometries of cracks. The effects of converging

Table 3. Error data from the comparison between models and experiments

Model \ Experimental data	Collier *et al.*, simulated cracks		Collier *et al.*, real cracks		Amos & Schrock, simulated cracks		Present work, real cracks		Present work, simulated cracks	
	$\bar{X}_m$(%)	S_{Rm}(%)	$\bar{X}_m$(%)	S_{Rm}(%)	$\bar{X}$m(%)	S_{Rm}(%)	$\bar{X}_m$(%)	S_{Rm}(%)	$\bar{X}_m$(%)	S_{Rm}(%)
Collier *et al.*	−16	62	27	62	56	63	−41	51	33	39
Abdollahian Model I	(6)	49	(−15)	97	22	29	−78	91	10	20
Abdollahian Model II	−8	(48)	16	(59)	31	38	−55	79	10	30
Modified Pana Model	−49	108	55	92	(9)	(21)	(−24)	(27)	(6)	(14)
No. of experimental points	27		70		345		100		358	
(%)	(3)		(8)		(38)		(11)		(40)	

and diverging cross-sections as well as the influence of the surface structures, caused for instance by different break mechanisms (intergranular stress corrosion cracks etc.), were not studied.

Acknowledgements—We are very grateful to St. Müller and Professor Dr D. Munz for their assistance in producing the real cracks and to G. Eisele and L. Pawlak for operating the test facility.

REFERENCES

ABDOLLAHIAN, D. 1983 Calculation of leak rates through cracks in pipes and tubes. Report EPRI NP-3395.

ABDOLLAHIAN, D. 1984 Analytical prediction of single-phase and two-phase flow through cracks in pipes and tubes. In *Proc. Heat Transfer—Niagara Falls. AIChE Symp. Ser.* **80,** No. 236, 19–23.

AMOS, C. N. & SCHROCK, V. E. 1983 Critical discharge of initially subcooled water through slits. Report NUREG/CR-3475.

BUTTON, B. L., GROGAN, A. F., CHIVERS, T. C. & MANNING, P. R. 1978 Gas flow through cracks. *J. Fluids Engng* **100,** 453–458.

COLLIER, R. P., LIU, J. S., MAYFIELD, M. E. & STUBEN, F. B. 1980 Study of critical two-phase flow through simulated cracks. Report BCL-EPRI-80-1.

COLLIER, R. P., STUBEN, F. B., MAYFIELD, M. E., PAPE, D. B. & SCOTT, P. M. 1984 Two-phase flow through intergranular stress corrosion cracks. Report EPRI-NP-3540-LD. Research Project T118-2, Final Report.

FRIEDEL, L. 1985 Siedeverzug in Kältemitteln bei plötzlicher Druckentlastung aus dem Gleichgewichtszustand. *Chem.-Ing.-Tech.* **57,** 154/155.

HENRY, R. E. 1970a The two-phase critical discharge of initially saturated or subcooled liquid. *Nucl. Sci. Engng* **41,** 336–342.

HENRY, R. E. 1970b An experimental study of low-quality, steam–water critical flow at moderate pressures. Report ANL-7740.

HENRY, R. E. & FAUSKE, H. K. 1971 The two-phase critical flow of one-component mixtures in nozzles, orifices and short tubes. *Trans. ASME, J. Heat Transfer* **95,** 179–187.

JOHN, H., REIMANN, J. & EISELE, G. 1987 Kritische Leckströmung aus rauhen Rissen in Druckwasserbehältern. Report KfK 4192.

KEFER, V., KASTNER, W. & KRÄTZER, W. 1986 Leckraten bei unterkritischen Rohrleitungsrissen. Jahrestagung Kerntechnik, Aachen.

LEVY, S. 1982 Homogeneous non-equilibrium critical flow model. *Int. J. Heat Mass Transfer* **25,** 16, 759/770.

MOODY, F. J. 1965 Maximum flowrate of a single component two-phase mixture. *Trans. ASME, J. Heat Transfer* **87,** 134–142.

MÜLLER, H. M., MÜLLER, S., MUNZ, D. & NEUMANN, J. 1986 Extension of surface cracks during cyclic loading. In *Fracture Mechanics*, Vol. 17 (ASTM STP 905), pp. 625–643. American Society for Testing and Materials, Philadelphia, Pa.

MUNZ, D. 1984 Leck-vor-Bruch-Verhalten druckbeaufschlagter Komponenten. Fortschr.-Ber. *VDI-Z.* **18,** No. 14.

NIKURADSE, J. 1933 Strömungsgesetze in rauhen Rohren. *VDI ForschHft* 361.

PANA, P. 1975 Eine modifizierte Bernoulli-Gleichung für die Berechnung der Strömungsvorgänge im unterkühlten Wassergebiet. Report IRS-W-18.

PANA, P. 1976 Berechnung der stationären Massenstromdichte von Wasserdampfgemischen und der auftretenden Rückstoßkräfte. Report IRS-W-24.

REIMANN, J. 1984 Vergleich von kritischen Massenstrommodellen im Hinblick auf die Strömung durch Lecks. Fortschr.-Ber. *VDI-Z.* **18,** No. 14, 63–94.

SCHLICHTING, H. 1955 *Boundary Layer Theory*. Pergamon Press, Oxford.

VDI-Wärmeatlas 1984 *4. Auflage*, LC 2. VDI-Verlag, Düsseldorf.

WALLIS, G. B. 1980 Critical two-phase flow. *Int. J. Multiphase Flow* **6,** 97–112.

ZALOUDEK, F. R. 1964 Steam–water critical flow from high pressure systems. Report HW-80535, Hanford Atomic Products Operation Richland, Wash.